Letter

Magneto-Seebeck coefficient of the Fermi liquid in three-dimensional Dirac and Weyl semimetals

F. R. Pratama [1,*] Riichiro Saito [2] and Nguyen T. Hung [2,3,†]

[1]*Mathematics for Advanced Materials-OIL, AIST, 2-1-1 Katahira, Aoba, 980-8577 Sendai, Japan*

[2]*Department of Physics, Tohoku University, Sendai 980-8578, Japan*

[3]*Frontier Research Institute for Interdisciplinary Sciences, Tohoku University, Sendai 980-8578, Japan*

(Received 17 June 2022; revised 11 August 2022; accepted 18 August 2022; published 31 August 2022)

We investigate dissipationless magneto-Seebeck effect in three-dimensional Dirac and Weyl semimetals. The Hall resistivity ρ_{yx} and thermoelectric Hall coefficient α_{xy} exhibit plateaus at the quantum limit, where electrons occupy only the zeroth Landau level. In this condition, quantum oscillation in the Seebeck coefficient $S_{xx} \approx \rho_{yx}\alpha_{xy}$ is suppressed, and the massless fermions are transformed into a Fermi liquid system. We show that the Seebeck coefficient at the quantum limit is expressed by the harmonic sum of Fermi wavelength and thermal de Broglie wavelength scaled by magnetic length.

DOI: 10.1103/PhysRevB.106.L081304

Research on thermoelectricity in low-dimensional materials is pioneered by the theoretical works of Hicks and Dresselhaus [1–3]. They found that by reducing the dimension of materials (essentially confining charge carriers in one or two directions), a larger Seebeck coefficient S_{xx} (or thermopower) and power factor can be obtained due to enhancement of electronic density of states (DOS) at the Fermi energy. Such a quantum confinement effect takes place only if the typical size of the material is smaller than the thermal de Broglie (TDB) wavelength [4–6]. In this Letter, we show that an analogous phenomenon also occurs in three-dimensional (3D) Dirac and Weyl semimetals when we apply magnetic field B. The confinement of massless fermions in a 3D Fermi pocket by B will induce the Fermi liquid behavior in the material.

An advantage of using 3D Dirac and Weyl semimetals in magnetothermoelectric devices was pointed out by Skinner and Fu [7]. They showed that a large, nonsaturating S_{xx} as a function of the magnetic field is achieved in the dissipationless limit. By keeping the number of carriers n_0 constant, the thermoelectric Hall coefficient over temperature α_{xy}/T approaches a finite value, and the Hall resistivity ρ_{yx} is expressed by the classical formula $\rho_{yx} = B/(n_0 e)$ (e is the elementary charge) [8–10]. Therefore, S_{xx} is linearly proportional to B, $S_{xx} \approx \rho_{yx}\alpha_{xy} \propto B$ [11]. On the other hand, Galeski *et al.* [12] recently observed saturating S_{xx} in a 3D Dirac semimetal $ZrTe_5$ [13], in which the classical ρ_{yx} no longer holds and 3D quantum Hall effect (QHE) occurs. They showed that the Hall plateau in the quantum limit is proportional to half of the Fermi wavelength in the direction parallel to the magnetic field, $\lambda_F^{\parallel}$, $\rho_{yx} \propto \lambda_F^{\parallel}/2$.

Similar experimental results are reported by Tang *et al.* [14] in $ZrTe_5$, and by Wang *et al.* [15] in $HfTe_5$. It is important to note that the QHE appears only in two-dimensional electron systems when the Fermi level is located between two Landau levels (LLs) [16,17]. Thus, 3D materials normally do not exhibit the QHE because of the continuous dispersion along the direction of B. To explain the QHE in 3D Dirac and Weyl semimetals, it was argued [14] that the formation of a charge density wave (CDW) [18,19] due to the Fermi surface instability plays a decisive role in discrete LLs near the Fermi energy. However, spectroscopic and transport measurements [12] do not show any signs of CDW. Thus, it is necessary to confirm analytically whether the Hall plateau arises from the intrinsic bulk properties of the 3D Dirac and Weyl fermions, especially since recent calculations on the magnetotransport coefficients of the Weyl semimetal with finite thickness do not show $\rho_{yx} \propto \lambda_F^{\parallel}/2$ in the quantum limit [20–23].

In this Letter, we show that the saturated value of S_{xx} is the Seebeck coefficient of 3D Fermi liquid $\mathcal{S}$ [24]. In particular, we show that the condition for $S_{xx} = \mathcal{S}$ follows a scaling law between three fundamental lengths: the magnetic length, the Fermi wavelength, and the TDB wavelength in the direction perpendicular to B, where carriers are magnetically confined. Further, we show that the QHE and saturating Seebeck coefficient originate from the occupation in the zeroth LL in the 3D Dirac fermion, which possesses a linear dispersion and is independent of B, and thus cannot be satisfied in electron gas in conventional 3D metals or semiconductors.

The calculation of the Hall conductivity and thermoelectric Hall coefficient is carried out within quantum edge formalism [7,8,25–27], where transport scattering time τ is assumed to be small compared with the inverse of cyclotron frequency $1/\omega_c$, i.e., $\omega_c\tau \gg 1$. In this condition, the magnitude of the longitudinal conductivity σ_{xx} is much smaller than σ_{xy}, which implies that the Hall resistivity is approximately given by $\rho_{yx} \approx 1/\sigma_{xy}$, and $S_{xx} \approx \alpha_{xy}/\sigma_{xy} = \rho_{yx}\alpha_{xy}$ [28].

Let us consider 3D Weyl and Dirac semimetals with a volume $L_xL_yL_z$, where L_i with $i = x, y, z$ is the length of the material in the ith direction. In the presence of an external magnetic field in the z-direction $\mathbf{B} = B\hat{\mathbf{z}}$, an electron is

*pratama.fr@aist.go.jp
†nguyen@flex.phys.tohoku.ac.jp

confined to move on an orbit in the xy plane, but move freely in the z direction with the Fermi velocity v_F^z. A potential difference V_x is applied between the right ($x = +L_x/2$) and left ($x = -L_x/2$) edges of the sample, which gives rise to the electric field $\mathbf{E} = E_x\hat{\mathbf{x}} = -\partial V_x/\partial x$. In the presence of both B and E_x, the LL spectrum without the Zeeman term is given by (see Sec. A in the Supplemental Material [29] with Refs. [30–32] for the derivation)

$$E_n(B, k_y, k_z) = \varepsilon_d(B, k_y) + \varepsilon_n(B, k_z), \tag{1}$$

where $\varepsilon_d(k_y) \equiv \hbar k_y v_d$ and $\varepsilon_n(k_z) \equiv \mathrm{sgn}(n)\sqrt{{\mathcal{E}_B}^2|n|/\gamma^3 + (\hbar v_F^z k_z/\gamma)^2}$. Because of $\varepsilon_d(k_y)$, the LL is dispersive along k_y, which allows charge carriers to move in the y direction with velocity $v_y = \hbar^{-1}\partial E_n(k_y, k_z)/\partial k_y = v_d$, where $v_d \equiv E_x/B$ is the drift velocity. $\varepsilon_n(k_z)$ corresponds to the cyclotron energy, where $\mathcal{E}_B \equiv \sqrt{2}\hbar v_F^\perp/\ell_B$, $\ell_B \equiv \sqrt{\hbar/(eB)}$ is the magnetic length, and $v_F^\perp$ is the Fermi velocity in the direction perpendicular to the magnetic field. Due to the relativistic nature of the Dirac fermion, the effect of E_x is also included in the Lorentz factor, $\gamma \equiv 1/\sqrt{1-(v_d/v_F^\perp)^2}$, which induces the shrinking of the LL for $E_x \neq 0$ [30,31]. Nevertheless, since we focus on the case for strong B, we can take $\gamma \approx 1$. It is noted that for $|k_z| \neq 0$, there are two possible values of the zeroth LL, i.e., $E_0 = \varepsilon_d(k_y) \pm \hbar v_F^z k_z$.

By using the fact that $\ell_B \ll L_z$, $k_z = 2\pi n_z/L_z$ ($n_z \in \mathbb{Z}$) can be treated as a continuous variable $\sum_{k_z}/L_z \to \int_0^\infty dk_z/\pi$, the DOS per unit volume for each spin direction is given by

$$\mathcal{D}(E) = \frac{eB}{h}\sum_{k_y}\int_0^\infty \frac{dk_z}{\pi}\sum_{n=-\infty}^{\infty} N_n\delta[E - E_n(k_y, k_z)], \tag{2}$$

where we define $N_n \equiv 1/2$ (1) for $n = 0$ ($n \neq 0$) to avoid double counting of the zeroth LL that includes both the plus and minus signs of E_0. The number of charge carriers n_0 is given by the difference between the number of electrons and holes, as follows:

$$n_0 = \int_0^\infty dE\mathcal{D}(E)f(E-\mu^*) - \int_{-\infty}^0 dE\mathcal{D}(E)[1-f(E-\mu^*)], \tag{3}$$

where $f(E-\mu^*) \equiv 1/[e^{\beta(E-\mu^*)}+1]$ is the Fermi-Dirac distribution function, $\beta \equiv 1/(k_B T)$. The chemical potential μ^* is given as a function of x due to V_x:

$$\mu^*(x) = \mu + eV_x x/L_x, \tag{4}$$

where μ is a term which determines the average carrier density [33] in the sample. Hereafter, we adopt the condition that μ in Eq. (4) is kept constant with respect to magnetic field.

For a given n_0 in Eq. (3), the electrical J_y and heat J_y^Q currents are given by [8]

$$\begin{pmatrix} J_y \\ J_y^Q \end{pmatrix} = v_y n_0 \begin{pmatrix} -e \\ E-\mu^* \end{pmatrix} = -E_x \begin{pmatrix} \sigma_{xy} \\ T\alpha_{xy} \end{pmatrix}. \tag{5}$$

By considering only the currents along the edges ($x = \pm L_x/2$), σ_{xy} and α_{xy} in Eq. (5) are given as a function of μ and T, as follows (see Secs. C and D in the Supplemental Material [29] with Refs. [20,33–37] for derivation):

$$\sigma_{xy} = \frac{2e^2}{h}\sum_{j=\pm1}\sum_{n=0}^{\infty} jN_n\int_0^\infty \frac{dk_z}{\pi} f[\varepsilon_n(B,k_z) - j\mu] \equiv \sigma_{xy}^{(0)} + \sum_{n=1}^{\infty}\sigma_{xy}^{(n)}, \tag{6}$$

and

$$\alpha_{xy} = \frac{2ek_B}{h}\sum_{j=\pm1}\sum_{n=0}^{\infty} N_n\int_0^\infty \frac{dk_z}{\pi}\left\{\ln[1+e^{-\beta\{\varepsilon_n(B,k_z)-j\mu\}}] + \frac{\beta[\varepsilon_n(B,k_z)-j\mu]}{e^{\beta[\varepsilon_n(B,k_z)-j\mu]}+1}\right\} \equiv \alpha_{xy}^{(0)} + \sum_{n=1}^{\infty}\alpha_{xy}^{(n)}, \tag{7}$$

where $\sigma_{xy}^{(n)}$ and $\alpha_{xy}^{(n)}$ denote, respectively, the Hall conductivity and thermoelectric Hall coefficient for the nth LL. The prefactor of 2 in Eqs. (6) and (7) is given by assuming that filling factors of the LL at $x = \pm L_x/2$ are the same [34,35], where almost symmetrical currents at the both edges flow in the same direction [33,36]. The index $j = +1$ and -1 indicate the contributions of electron and hole, respectively. $\sigma_{xy}^{(0)}$ and $\alpha_{xy}^{(0)}$ are the Hall conductivity and thermoelectric Hall coefficient for the zeroth LL, which are obtained analytically as follows:

$$\sigma_{xy}^{(0)} = \frac{2e^2}{h^2 v_F^z \beta}\sum_{j=\pm1} j\ln(1+e^{j\beta\mu}), \tag{8}$$

and

$$\alpha_{xy}^{(0)} = \frac{-2ek_B}{h^2 v_F^z}\sum_{j=\pm1}\left[\frac{2}{\beta}\mathrm{Li}_2(-e^{j\beta\mu}) + j\mu\ln(1+e^{j\beta\mu})\right], \tag{9}$$

where $\mathrm{Li}_2(z) \equiv \sum_{k=1}^\infty z^k/k^2$ is the dilogarithm function.

Hereafter, we adopt the parameters for calculating $\rho_{yx} = 1/\sigma_{xy}$ and α_{xy} from the experimentally determined values of 3D Dirac semimetal $ZrTe_5$ [12]. The material has an orthorombic crystal structure and anisotropic Fermi velocities v_F^i along $i = a$, b, and c axis, where $v_F^a = 1.164 \times 10^5$ m/s, $v_F^b = 1.534 \times 10^4$ m/s, and $v_F^c = 3.489 \times 10^5$ m/s. By aligning B parallel to the b axis, the Fermi wave vector $k_F^b = 72.9 \times 10^{-3}$ Å^{-1} is extracted from the Hall plateau in the quantum limit, where only the zeroth LL is occupied. To reproduce the experimental measurement of ρ_{yx} with our model, we use $k_F^z = k_F^b$, $v_F^z = v_F^b$, $v_F^\perp = \sqrt{v_F^a v_F^c} = 2.015 \times 10^5$ m/s, and $\mu = \hbar v_F^z k_F^z = 7.36$ meV. In the dissipationless limit, the typical value of E_x is 2×10^2 V/m [35]. Here, we adopt the smallest value of $B = 10^{-2}$ T. Thus, $v_d \approx 10^4$ m/s and the approximation $\gamma \equiv 1/\sqrt{1-(v_d/v_F^\perp)^2} \approx 1$ in Eq. (1) is valid. Furthermore, at the corresponding B, the magnetic length becomes $\ell_B = 2.566\,\mu$m, which is much smaller than the thickness of the $ZrTe_5$ sample ($L_z \sim 10^2\,\mu$m) used in the

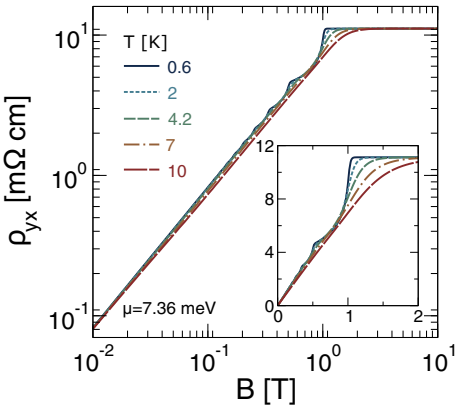

FIG. 1. Log-log plot of ρ_{yx} as a function of B at a constant $\mu = 7.36\,\text{meV}$ for several values of T. Inset shows the linear plot of ρ_{yx} for $B = 0 - 2\,\text{T}$.

experiment [12]. For the corresponding L_z, we do not consider the role of the Fermi arcs, which is essential to support 3D QHE when L_z is comparable to the mean-free path ($\sim$100 nm) by forming a closed Fermi loop [38]. It is because (1) we consider a single Dirac point in the Brillouin zone and (2) L_z is much larger than the mean-free path.

In Fig. 1, we show a log-log plot of ρ_{yx} as a function of B for $T = 0.6, 2, 4.2, 7$, and 10 K. For all temperatures, the quantum Hall regime occurs at $B \sim 1\,T$, as shown in the inset of Fig. 1. It is noted that the quantization of ρ_{yx} is not as pronounced as in the two-dimensional case due to the logarithmic singularity of the DOS upon the integration on k_z (see Sec. B in the Supplemental Material [29]). As we further increase B, ρ_{yx} becomes independent of B and T, which indicates that all $n > 0$ LLs are depopulated. As shown in the inset of Fig. 1, the Hall plateau at $\rho_{xy} \approx 11.6\,\text{m}\Omega\,\text{cm}$ occurs for $B \geqslant 1.2\,\text{T}$. The present calculation reproduces recent experiments by Tang [14] and Galeski [12]. The good agreement can be attributed to small effective mass in $ZrTe_5$ [12,14,39–41] (in the order of $\sim 0.01 m_e$, where m_e is the mass of free electron), and because there is only one spin degeneracy for each zeroth LL [13,42,43].

Let us discuss the quantum limit case, in which $\rho_{yx} = 1/\sigma_{xy}^{(0)}$. From Eq. (8), the term at $j = -1$ vanishes for low temperature ($|\mu\beta| \gg 1$), which means that only electrons contribute to the constant ρ_{yx} for $\mu > 0$ (and holes for $\mu < 0$ but with opposite sign of ρ_{yx}). By using $\ln(1 + e^{\beta\mu}) \approx \beta\mu$, ρ_{yx} is independent of T as follows:

$$\rho_{yx} = \frac{2e^2\mu}{h^2 v_F^z} = \frac{\pi h}{e^2 k_F^z} = \frac{h\lambda_F^z}{2e^2}, \tag{10}$$

where $\lambda_F^z = 2\pi/k_F^z \equiv \lambda_F^{\parallel}$. It is noted that the magnitude of the Hall plateau shown by Eq. (10) has been confirmed experimentally in the samples of $ZrTe_5$ with thickness $L_z \approx 100\,\mu\text{m}$, while an experiment on the 2D Dirac semimetal Cd_3As_2 [44] with $L_z \approx 60 - 70\,\text{nm}$ does not indicate such behavior. Thus, we show that Eq. (10) is indeed an intrinsic property of 3D Dirac semimetal.

In Figs. 2(a) and 2(b), we show log-log plots of α_{xy} and $S_{xx} = \rho_{yx}\alpha_{xy}$ as a function of B for $T = 0.6, 2, 4.2, 7$, and 10 K, respectively. We can see that for $B \leqslant 1\,\text{T}$, α_{xy} de-

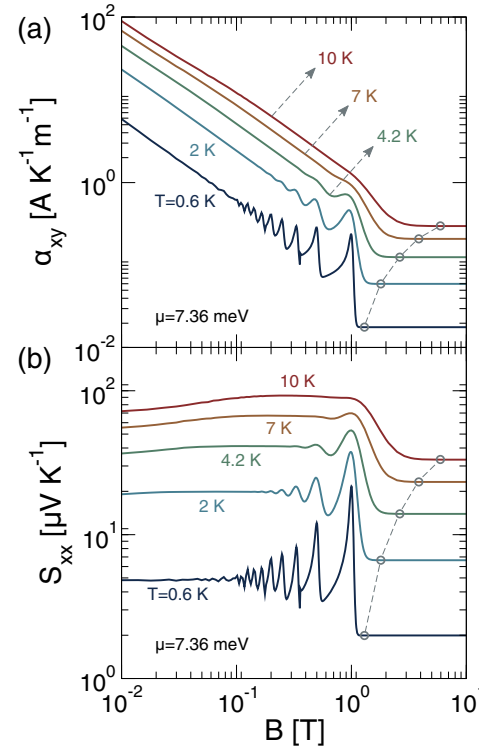

FIG. 2. Log-log plot of (a) α_{xy} and (b) S_{xx} as a function of B for several values of T. The chemical potential is set at $\mu = 7.36\,\text{meV}$. Grey circles indicate the saturated magnetic field, where α_{xy} and S_{xx} begin to saturate.

creases linearly with increasing B, which means that α_{xy} is inversely proportional to B in the linear scale. On the other hand, S_{xx} does not show significant dependence on B. As B becomes larger, oscillations appears in both α_{xy} and S_{xx} for $T \leqslant 4.2\,\text{K}$ since a few LLs touch the chemical potential. Due to the smearing of the Fermi-Dirac distribution function by increasing T, the individual peaks in the oscillation become indistinguishable. As the quantum limit takes place, α_{xy} and S_{xx} become constants for all temperatures. By applying the identity $\text{Li}_2(z) + \text{Li}_2(1/z) = -\pi^2/6 - [\ln(-z)]^2/2$ on Eq. (9), the explicit formula for thermoelectric Hall plateau $\alpha_{xy} = \alpha_{xy}^{(0)}$ is given as follows:

$$\alpha_{xy} = \frac{2\pi^2}{3}\frac{e{k_B}^2}{h^2 v_F^z}T. \tag{11}$$

Equation (11) was first obtained by Kozii *et al.* [8] as the saturating limit for α_{xy} of an ideal 3D Dirac semimetal at a large B, with a fixed number of carriers. We complement the result by showing that exactly the same formula also prevails for a fixed chemical potential. By combining Eqs. (10) and (11), S_{xx} at the quantum limit is given as follows:

$$S_{xx} = \frac{\pi^2}{3}\frac{{k_B}^2}{e}\frac{T}{\mu} \equiv \mathcal{S}, \tag{12}$$

where $\mathcal{S}$ is the expression for the Seebeck coefficient of the Fermi liquid system [24].

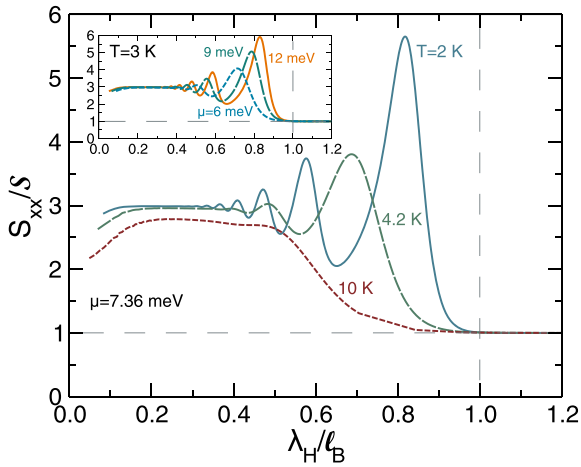

FIG. 3. Plot of the scaled Seebeck coefficient $S_{xx}/\mathcal{S}$ as a function of λ_H/ℓ_B for constant $\mu = 7.36$ meV for several values of T. Inset: $S_{xx}/\mathcal{S}$ at a constant $T = 3$ K for several values of μ.

Now, let us discuss the onset of magnetic field in which the 3D Dirac and Weyl materials behave as the Fermi liquid system at the saturated magnetic field (open circles in Fig. 2). It is noted that in the quantum limit, the uncertainty principle determines that the radius of the electron's orbit is given by the magnetic length ℓ_B. Therefore, it is useful to express the dependence of the saturated magnetic field in term of the length scales associated with μ and T in the direction perpendicular to B where magnetic confinement of electrons occurs. At $T = 0$ K, the plateau is formed when the magnetic energy is larger than the chemical potential, i.e., $\mathcal{E}_B \geqslant \mu$ with $\mu = \hbar v_F^{\perp} k_F^{\perp} = h v_F^{\perp}/\lambda_F^{\perp}$. Thus, $T \cong 0$ K, S_{xx} becomes $\mathcal{S}$ when the ratio of the two length scales satisfies $\ell_B/\lambda_F^{\perp} \leqslant 1/(\sqrt{2}\pi) \approx 0.225$.

For given a finite T, σ_{xy} and α_{xy} are obtained by a convolution of $-\partial f(E-\mu, T)/\partial E = (\beta/4)\mathrm{sech}^2[\beta(E-\mu)/2]$ with those quantities at $T = 0$ K (see the Supplemental Material [29]). Thus, the shift from $\ell_B/\lambda_F^{\perp}$ is given by $W = 2k_B T/\mathcal{E}_B$, resulting in Eq. (12) holding if the following condition is satisfied:

$$\frac{\ell_B}{\lambda_F^{\perp}} + W \leqslant \frac{1}{\sqrt{2}\pi}. \tag{13}$$

The length scale associated with the temperature is TDB wavelength [6]. We adopt a definition of the TDB wavelength [45] which is suitable for massless particle $\Lambda^{\perp} \equiv h v_F^{\perp}/(2\pi^{1/3} k_B T)$. Equivalently, $W = \sqrt{2}\pi^{2/3}\ell_B/\Lambda^{\perp}$. By defining $1/\lambda_H$ as a weighted harmonic sum of $\lambda_F^{\perp}$ and $\Lambda^{\perp}$,

$$\frac{1}{\lambda_H} \equiv \frac{\sqrt{2}\pi}{\lambda_F^{\perp}} + \frac{2\pi^{5/3}}{\Lambda^{\perp}}, \tag{14}$$

the condition for obtaining $S_{xx} = \mathcal{S}$ is given by $\lambda_H/\ell_B \geqslant 1$. In Fig. 3, we plot $S_{xx}/\mathcal{S}$ with $\mu = 7.36$ meV for $T = 2$, 4.2, and 10 K. Here, we can see the suppression of quantum oscillation for $\lambda_H/\ell_B \geqslant 1$. In Fig. 3, $\Lambda^{\perp}$ is varying while $\lambda_F^{\perp}$ remains constant. For the opposite condition, we plot S_{xx}/S for $\mu = 6$, 9, and 12 K at a constant $T = 3$ K (see inset plot in Fig. 3), where similar behavior is observed. This phenomenon shows that the confinement within the length of ℓ_B will transform the 3D Dirac fermions into a Fermi liquid system. In other words, the states of the Dirac fermions at the zeroth LL become localized in the k space within a small Fermi surface (due to low carrier density n_0), which does not change with keeping the chemical potential constant. When the magnetic field is large, the Coulomb interactions between electrons decreases because of the magnetic confinement. Thus, the magnetic confinement effectively transforms the Fermi surface into a weakly interacting regime. This explains the Fermi liquid behavior of the Dirac fermion in the quantum limit. In contrast, we show in Sec. E of the Supplemental Material [29] with Refs. [12,46,47] that for an ordinary massive 3D electron gas with a fixed μ, ρ_{yx} tends to increase after $n = 1$ LL is unoccupied, while α_{xy} becomes zero, thus 3D electron gas does not become the Fermi liquid at a strong magnetic field.

Finally, we have to consider the ranges of B and T in which the Fermi liquid phase can survive. For $\lambda_H/\ell_B \leqslant 1.2$ in Fig. 3, the maximum value of B is around 6 T for $T \leqslant 10$ K and $\mu \leqslant 12$ meV. Around this B and higher, the scaling law may be broken if the Zeeman term becomes more noticeable, especially if the material has a large g factor. This may explain the increase of ρ_{xy} in $ZrTe_5$ [12,14] and $HfTe_5$ [15] for $B \geqslant 3$ T though the Hall plateaus are observed for $B < 3$ T. In these materials, the value of g is in the order $\sim$10 [12,39,43,48]. It also has been observed that large B can drive phase transitions such as band inversion [42,49], anomalous QHE [48], as well as fractional QHE [14] and mass generation [50] due to many body interactions. Also at higher temperature, the transport becomes dissipative due to scattering effects [9,51], where ρ_{xx} increases and, as a consequence, the relation $S_{xx} \approx \rho_{yx}\alpha_{xy}$ is no longer valid. Nevertheless, our proposed scaling law for an ideal 3D Dirac material may be observed experimentally within proper ranges of B and T.

In summary, we have analytically shown that at a fixed chemical potential, both the Hall resistivity and thermoelectric Hall coefficient show plateau structures. In this condition, magnetic confinement of carriers occupying the zeroth LL transform the 3D Dirac and Weyl fermions into the Fermi liquid. Particularly, the threshold of this phenomenon can be parameterized by magnetic length, the Fermi wavelength, and the TDB wavelength. Our findings establish a relationship between the three fundamental lengths in the quantum Hall and thermoelectric Hall effects in the 3D Dirac/Weyl semimetals.

N.T.H. acknowledges JSPS KAKENHI (Grant No. JP20K15178) and financial support from the Frontier Research Institute for Interdisciplinary Sciences, Tohoku University. R.S. acknowledges JSPS KAKENHI Grants No. JP18H01810, No. JP22H00283 and CSIS, Tohoku University. F.R.P. thanks Dr. E. H. Hasdeo for a useful discussion.

[1] L. D. Hicks and M. S. Dresselhaus, Phys. Rev. B **47**, 12727 (1993).

[2] L. D. Hicks and M. S. Dresselhaus, Phys. Rev. B **47**, 16631 (1993).

[3] J. P. Heremans, M. S. Dresselhaus, L. E. Bell, and D. T. Morelli, Nat. Nanotechnol. **8**, 471 (2013).

[4] N. T. Hung, E. H. Hasdeo, A. R. T. Nugraha, M. S. Dresselhaus, and R. Saito, Phys. Rev. Lett. **117**, 036602 (2016).

[5] N. T. Hung, A. R. T. Nugraha, and R. Saito, Phys. Rev. Applied **9**, 024019 (2018).

[6] N. T. Hung and R. Saito, Adv. Quantum Technol. **4**, 2000115 (2021).

[7] B. Skinner and L. Fu, Sci. Adv. **4**, eaat2621 (2018).

[8] V. Kozii, B. Skinner, and L. Fu, Phys. Rev. B **99**, 155123 (2019).

[9] F. Han, N. Andrejevic, T. Nguyen, V. Kozii, Q. T. Nguyen, T. Hogan, Z. Ding, R. Pablo-Pedro, S. Parjan, B. Skinner *et al.*, Nat. Commun. **11**, 6167 (2020).

[10] W. Zhang, P. Wang, B. Skinner, R. Bi, V. Kozii, C.-W. Cho, R. Zhong, J. Schneeloch, D. Yu, G. Gu *et al.*, Nat. Commun. **11**, 1046 (2020).

[11] See generalizations of this result for massive [V. Könye and M. Ogata, Phys. Rev. B **100**, 155430 (2019)], compensated; [X. Feng and B. Skinner, Phys. Rev. Materials **5**, 024202 (2021)], and multi-3D Dirac/Weyl semimetals; [L. X. Fu and C. M. Wang, Phys. Rev. B **105**, 035201 (2022)].

[12] S. Galeski, T. Ehmcke, R. Wawrzyńczak, P. M. Lozano, K. Cho, A. Sharma, S. Das, F. Küster, P. Sessi, M. Brando *et al.*, Nat. Commun. **12**, 3197 (2021).

[13] R. Y. Chen, Z. G. Chen, X. Y. Song, J. A. Schneeloch, G. D. Gu, F. Wang, and N. L. Wang, Phys. Rev. Lett. **115**, 176404 (2015).

[14] F. Tang, Y. Ren, P. Wang, R. Zhong, J. Schneeloch, S. A. Yang, K. Yang, P. A. Lee, G. Gu, Z. Qiao, and L. Zhang, Nature (London) **569**, 537 (2019).

[15] P. Wang, Y. Ren, F. Tang, P. Wang, T. Hou, H. Zeng, L. Zhang, and Z. Qiao, Phys. Rev. B **101**, 161201(R) (2020).

[16] H. L. Störmer, J. P. Eisenstein, A. C. Gossard, W. Wiegmann, and K. Baldwin, Phys. Rev. Lett. **56**, 85 (1986).

[17] B. I. Halperin, Jpn. J. Appl. Phys. **26**, 1913 (1987).

[18] D. Sehayek, M. Thakurathi, and A. A. Burkov, Phys. Rev. B **102**, 115159 (2020).

[19] F. Qin, S. Li, Z. Z. Du, C. M. Wang, W. Zhang, D. Yu, H.-Z. Lu, and X. C. Xie, Phys. Rev. Lett. **125**, 206601 (2020).

[20] M. Chang, H. Geng, L. Sheng, and D. Y. Xing, Phys. Rev. B **103**, 245434 (2021).

[21] M. Chang and L. Sheng, Phys. Rev. B **103**, 245409 (2021).

[22] R. Ma, D. N. Sheng, and L. Sheng, Phys. Rev. B **104**, 075425 (2021).

[23] F. Xiong, C. Honerkamp, D. M. Kennes, and T. Nag, Phys. Rev. B **106**, 045424 (2022).

[24] K. Behnia and H. Aubin, Rep. Prog. Phys. **79**, 046502 (2016).

[25] B. I. Halperin, Phys. Rev. B **25**, 2185 (1982).

[26] S. M. Girvin and M. Jonson, J. Phys. C: Solid State Phys. **15**, L1147 (1982).

[27] D. L. Bergman and V. Oganesyan, Phys. Rev. Lett. **104**, 066601 (2010).

[28] K. von Klitzing, Rev. Mod. Phys. **58**, 519 (1986).

[29] See Supplemental Material at http://link.aps.org/supplemental/10.1103/PhysRevB.106.L081304 for the detailed derivation of the energy dispersion, density of states, Hall conductivity, and thermoelectric Hall coefficient of the 3D Driac and Weyl semimetals in Secs. A– D, respectively, and the Hall conductivity and thermoelectric Hall coefficient of the 3D electron gas in Sec. E. Refs. [12,20,27,30–37,46,47].

[30] N. Peres and E. V. Castro, J. Phys.: Condens. Matter **19**, 406231 (2007).

[31] V. Arjona, E. V. Castro, and M. A. H. Vozmediano, Phys. Rev. B **96**, 081110(R) (2017).

[32] V. Lukose, R. Shankar, and G. Baskaran, Phys. Rev. Lett. **98**, 116802 (2007).

[33] R. R. Gerhardts, K. Panos, and J. Weis, New J. Phys. **15**, 073034 (2013).

[34] M. E. Cage, J. Res. Natl. Inst. Stand. Technol. **102**, 677 (1997).

[35] K. Panos, R. R. Gerhardts, J. Weis, and K. von Klitzing, New J. Phys. **16**, 113071 (2014).

[36] P. Haremski, M. Mausser, A. Gauß, K. von Klitzing, and J. Weis, Phys. Rev. B **102**, 205306 (2020).

[37] V. P. Gusynin and S. G. Sharapov, Phys. Rev. Lett. **95**, 146801 (2005).

[38] C. M. Wang, H. P. Sun, H. Z. Lu, and X. C. Xie, Phys. Rev. Lett. **119**, 136806 (2017).

[39] Y. Jiang, Z. L. Dun, H. D. Zhou, Z. Lu, K. W. Chen, S. Moon, T. Besara, T. M. Siegrist, R. E. Baumbach, D. Smirnov, and Z. Jiang, Phys. Rev. B **96**, 041101(R) (2017).

[40] G. Zheng, J. Lu, X. Zhu, W. Ning, Y. Han, H. Zhang, J. Zhang, C. Xi, J. Yang, H. Du, K. Yang, Y. Zhang, and M. Tian, Phys. Rev. B **93**, 115414 (2016).

[41] J. Wang, J. Niu, B. Yan, X. Li, R. Bi, Y. Yao, D. Yu, and X. Wu, Proc. Natl. Acad. Sci. USA **115**, 9145 (2018).

[42] J. L. Zhang, C. M. Wang, C. Y. Guo, X. D. Zhu, Y. Zhang, J. Y. Yang, Y. Q. Wang, Z. Qu, L. Pi, H. Z. Lu, and M. L. Tian, Phys. Rev. Lett. **123**, 196602 (2019).

[43] Z.-G. Chen, R. Chen, R. Zhong, J. Schneeloch, C. Zhang, Y. Huang, F. Qu, R. Yu, Q. Li, G. Gu *et al.*, Proc. Natl. Acad. Sci. USA **114**, 816 (2017).

[44] C. Zhang, Y. Zhang, X. Yuan, S. Lu, J. Zhang, A. Narayan, Y. Liu, H. Zhang, Z. Ni, R. Liu *et al.*, Nature (London) **565**, 331 (2019).

[45] Z. Yan, Eur. J. Phys. **21**, 625 (2000).

[46] F. W. Olver, D. W. Lozier, R. F. Boisvert, and C. W. Clark, *NIST Handbook of Mathematical Functions* (New York, Cambridge University Press, 2010)

[47] R. Wawrzyńczak, S. Galeski, J. Noky, Y. Sun, C. Felser, and J. Gooth, Sci. Rep. **12**, 2153 (2022).

[48] Y. Liu, H. Wang, H. Fu, J. Ge, Y. Li, C. Xi, J. Zhang, J. Yan, D. Mandrus, B. Yan *et al.*, Phys. Rev. B **103**, L201110 (2021).

[49] G. Zheng, X. Zhu, Y. Liu, J. Lu, W. Ning, H. Zhang, W. Gao, Y. Han, J. Yang, H. Du, K. Yang, Y. Zhang, and M. Tian, Phys. Rev. B **96**, 121401(R) (2017).

[50] Y. Liu, X. Yuan, C. Zhang, Z. Jin, A. Narayan, C. Luo, Z. Chen, L. Yang, J. Zou, X. Wu *et al.*, Nat. Commun. **7**, 12516 (2016).

[51] X. Xu, Y. Liu, G. Seyfarth, A. Pourret, W. Ma, H. Zhou, G. Wang, Z. Qu, and S. Jia, Phys. Rev. B **104**, 115164 (2021).